

A statistical evaluation of the morphological variability of shortening landforms on Mercury



Stephan R. Loveless^{a,*}, Christian Klimczak^a, Leta R. McCullough^b, Kelsey T. Crane^b, Steven M. Holland^a, Paul K. Byrne^c

^a Department of Geology, University of Georgia, Athens, GA 30602, USA

^b Department of Geosciences, Mississippi State University, Mississippi State, MS 39762, USA

^c Department of Earth, Environmental, and Planetary Sciences, Washington University in St. Louis, St. Louis, MO, 63130, USA

ARTICLE INFO

Keywords:

Mercury
Tectonics
Tectonic geomorphology
Lobate scarp
Wrinkle ridge

ABSTRACT

Observations of Mercury from both the Mariner 10 and MESSENGER missions showed that Mercury has a global population of shortening landforms, with several thousands of individual structures identified to date. The accommodation of widespread tectonic shortening is widely regarded to be the result of global contraction—the long, sustained cooling of the interior that has caused the planet to shrink. Shortening landforms on Mercury have been traditionally categorized into three distinct categories: lobate scarps, wrinkle ridges, and high-relief ridges. Although the clearest examples of shortening landforms at the time were used to describe and define these categories qualitatively, later studies showed that shortening landforms on Mercury display morphological characteristics that do not make for a ready classification into one of these “traditional” groups. More recently, other studies have classified shortening landforms based on the terrain that those landforms reside in to avoid generalizing morphology. In this study, we quantitatively assess the shape of shortening landforms by measuring and compiling a suite of 12 morphological parameters for 100 such structures across the planet. These parameters were evaluated for their importance in defining categories using two multivariate statistical analyses, a Principal Component Analysis (PCA) and Linear Discriminant Analysis (LDA). These methods allow us to assess any correlation that the traditional categories, terrain types, or alternative classification schemes have with the variation observed across our set of measurements. Our results show that the morphologic characteristics of shortening landforms on Mercury are not accurately captured by traditionally recognized groups. Instead, shortening landforms fall along a morphological spectrum, where only a few ideal examples of lobate scarps or wrinkle ridges provide clear endmembers. Therefore, despite the frequent use of the terms “lobate scarps” and “wrinkle ridges” in works regarding planetary tectonics, we find that such terminology does not appropriately define the morphology of shortening landforms found on Mercury and may lead to the generalization, or misinterpretation of landforms described as accommodating shortening on Mercury’s surface. Future studies should test if a distinction between the landforms is found in the underlying thrust fault systems.

1. Introduction

1.1. Categories of shortening landforms

Modeling motivated by early observations from the Mariner 10 mission of crustal shortening had predicted that Mercury had undergone global contraction, a phenomenon resulting from the long, sustained cooling of a terrestrial body that leads to a planetary volumetric decrease (e.g., Solomon, 1977). Global contraction was predicted to be

principally accommodated via widespread thrust faulting throughout the brittle portion of Mercury’s lithosphere (Solomon, 1978) that manifests at the surface as linear, positive-relief landforms. Observations from the MErcury Surface, Space ENvironment, Geochemistry, and Ranging (MESSENGER) mission provided greater detail of the crustal shortening that accommodated global contraction (e.g., Byrne et al., 2014). In this study, we focus on these tectonic landforms related to global contraction. We use the strain term “shortening landforms” as an identifier of all positive-relief landforms we interpret as having been

* Corresponding author.

E-mail address: Stephan.Loveless@uga.edu (S.R. Loveless).

formed by thrust faulting; such landforms have been described as “shortening structures” or “thrust fault-related landforms” in earlier works but we prefer this term for consistency.

Mercury’s surface has been mapped into three main morphologic unit types: intercrater plains, smooth plains, and impact crater facies (e.g., Trask and Guest, 1975; Denevi et al., 2009; Denevi et al., 2013). Intercrater plains are heavily cratered and represent the oldest surfaces on the innermost planet. Smooth plains are interpreted to be more recently emplaced expanses of flood-volcanic deposits bearing fewer craters (Head et al., 2011; Denevi et al., 2013). Impact crater facies are collectively units that formed as direct or long-term consequences of large impacts, with most being contained within and around their host impact basins. Shortening landforms occur in all surface morphologic units (e.g., Byrne et al., 2014) and are interpreted to have acquired most of their strain near the end of when the smooth plains were emplaced and somewhat thereafter (Byrne et al., 2016, 2018; Crane and Klimczak, 2017).

Shortening landforms are not only found on Mercury but on all major terrestrial bodies. Generally, they are manifest as surface-breaking scarps showing positive relief (e.g., Schultz and Watters, 2001; Watters, 2003). Early photogeologic data sets of Mercury, Venus, the Moon, and Mars revealed shortening landforms with several typical characteristics (e.g., Strom et al., 1975). Strom et al. (1975) attributed the morphology of shortening landforms on Mercury to tectonic processes

and crater-forming events. Dzurisin (1978) initially categorized shortening landforms on Mercury into six morphological groups: arcuate scarps, lobate scarps, irregular intracrater scarps, irregular Caloris scarps, linear ridges, and irregular Caloris ridges. Of those, lobate scarps and wrinkle ridges were used to describe tectonics observed from the Mariner 10 mission (e.g., Strom, 1979) and were subsequently used widely to categorize shortening landforms throughout the Solar System, including Mercury (e.g., Melosh and McKinnon, 1988; Watters and Robinson, 1999; Watters et al., 2004), Venus (e.g., Solomon et al., 1992; Squyres et al., 1992), and Mars (e.g., Watters and Robinson, 1999; Mueller and Golombek, 2004). A few high-relief ridges have been described in detail on Mercury (Watters et al., 2001). In this paper, we refer to lobate scarps, wrinkle ridges, and high-relief ridges as the “traditional categories” by which extraterrestrial crustal shortening structures have been identified and mapped.

Lobate scarps (Fig. 1a) are linear to bow-like structures in map-view that have a surface break. In cross-section, they have asymmetric positive relief with a relatively steep sloping forelimb that immediately trails the surface break followed by a more gently sloping backlimb (e.g., Strom et al., 1975; Strom, 1979; Watters, 1993). The shapes of lobate scarps provide evidence that the vergence, or direction of tectonic transport, of the thrust system is in the direction of the forelimb with anticlinal folding of the hanging wall (e.g., Byrne et al., 2014). Named examples of lobate scarps on Mercury have the International

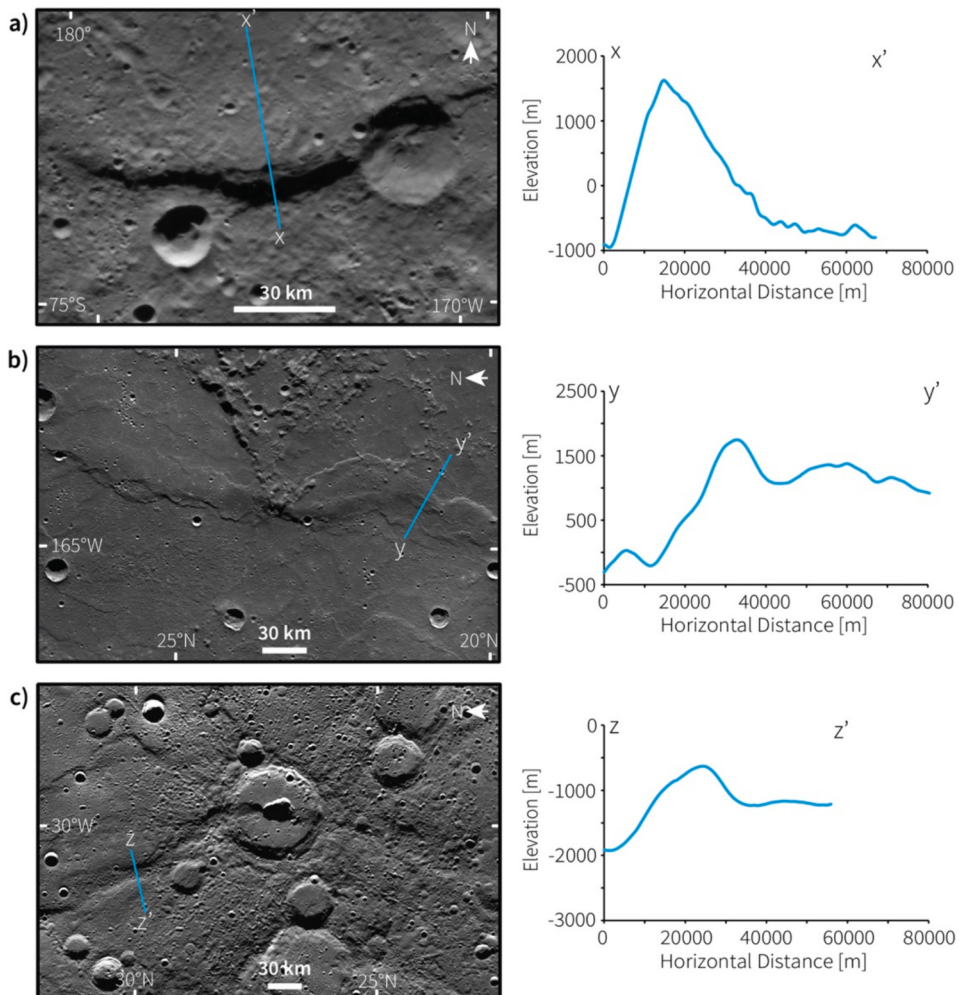


Fig. 1. Examples of the three “traditional” categories of shortening landforms found on Mercury. a) Map view of an unnamed lobate scarp near the south pole (left) along with the corresponding topographic profile from x to x'. b) The wrinkle ridge Schiaparelli Dorsum in map view (left) along with the corresponding topographic profile from y to y'. c) The high-relief ridge Antoniadi Dorsum in map view (left) and its corresponding topographic profile from z to z'. All images are shown in a stereographic projection centered on the shortening landform and all profiles are shown at ~16x vertical exaggeration.

Astronomical Union (IAU) descriptor term *rupes* (pl. “*rupēs*”) (e.g., Beagle *Rupes*, Enterprise *Rupes*, Carnegie *Rupes*, etc.).

Wrinkle ridges on Mercury (Fig. 1b) generally have lower relief than lobate scarps and differ from other shortening landforms by their complex, sinuous map pattern and their superimposed ridge (the “wrinkle”) above a primary broad ridge (e.g., Watters, 1988). Wrinkle ridges are common on the volcanic plains of many terrestrial bodies in the Solar System (e.g., Plescia and Golombek, 1986; Nahm et al., 2023). They are interpreted as anticlinal structures formed above blind thrust faults (e.g., Schultz, 2000) and potentially backthrusts (Okubo and Schultz, 2004); however, surface breaks are common (Strom et al., 1975; Watters, 1988; Golombek et al., 1991; Golombek et al., 2001; Schleicher et al., 2019).

High-relief ridges (Fig. 1c) have been reported by a single author on both Mercury and Mars (Watters, 1993), with only a few examples on the former. In cross-section, high-relief ridges are morphologically similar to lobate scarps but are more symmetric due to the landforms hosting a steeper backlimb (e.g., Watters et al., 2021). High-relief ridges have been interpreted to be anticlines formed above steeply dipping reverse faults (e.g., Watters et al., 2001).

Byrne et al. (2014) avoided using these traditional morphological categories and instead classified shortening landforms by the terrain type in which they are found. These authors’ classification includes smooth-plains structures, cratered-plains structures, crater-related structures, and high-terrain bounding structures. Crater-related structures are defined as landforms bound to and/or found within an impact basin, and high-terrain bounding structures are described as landforms separating high-standing from low-lying terrain. However, both of these structure types still occur in either smooth- or cratered-plains, and so the four categories in Byrne et al. (2014) can be further simplified to smooth-plains structures or cratered-plains structures.

1.2. Motivation and goal of this study

The traditional landform categories of lobate scarps, wrinkle ridges, and high-relief ridges are qualitative; no quantified definitions by which these landforms can be systematically classified or distinguished have been proposed. As Strom et al. (1975) stated regarding shortening landforms mapped around the Caloris basin using images from the Mariner 10 mission: “*Many of the scarps in the plains surrounding the Caloris Basin grade into or are transitional with ridges, so that the two structures are difficult to distinguish*”. Other studies of Mercury’s shortening landforms have questioned the traditional categories: although endmembers of the traditional categories are present, most structures are not so easily classified (e.g., Byrne et al., 2014; Byrne et al., 2018; Klimczak et al., 2018; Crane and Klimczak, 2019). We therefore carry out a statistical investigation of the morphology of the traditional categories of lobate scarps and wrinkle ridges on Mercury to establish whether there is a quantitative basis by which to use these traditional terms in studying the planet’s inventory of crustal shortening structures. To do so, we based our study on multivariate statistical analysis of morphologic measurements of select shortening landforms of each assessed type. This approach allowed us to not only evaluate whether the traditional categories can be distinguished, but also to assess other categorizations, such as those based on terrain types (e.g., those advocated by Byrne et al., 2014). We do not consider high-relief ridges in our assessment due to the low sample size of landforms in this category and the statistical inaccuracies that may arise as a result..

2. Methods

2.1. Data collection

The entire catalog of global image mosaics at a resolution of 166 m/pixel and digital elevation models (DEMs) from the MESSENGER mission available on the Planetary Data System (PDS) was loaded into a

Geographic Information System (GIS) using ArcMap® 10.8. This includes the 250 m/pixel northern hemisphere MLA DTM (Zuber et al., 2012). We also used the DEMs from MESSENGER flybys (Preusker et al., 2011) and the more recently resolved DEM of the south pole by Bertone et al. (2023) at a resolution 250 m/pixel. The lowest-resolution elevation dataset used in this study is the global USGS DEM, which is based on the Mercury Dual Imaging System narrow-angle camera and multispectral wide-angle camera and has a resolution of ~665 m/pixel (Becker et al., 2016). For coverage of topography see supplementary material (Loveless et al., 2024).

In ArcMap, Mercury was divided into a $20^\circ \times 20^\circ$ grid, producing 162 grid boxes, of which 100 were randomly selected with uniform probability via a random number generator. Each grid box was thoroughly surveyed for shortening landforms, and one such landform was then chosen based on what would be the best candidate with respect to the rest of the data collection. Selections were made to account for good representations of global distribution (see Fig. 2), size, traditional categories, and also DEM availability and resolution. If shortening landforms fell into an area with only the lower-resolution, global DEM topography, only large shortening landforms (>100 km long) were selected to minimize the effect of DEM spatial resolution on the topographic measurements.

Each selected landform was assigned a lobate scarp, wrinkle ridge, or transitional (i.e., a structure that transitions from a lobate scarp to a wrinkle ridge along its length) classification. High-relief ridges were not considered because only a small number have been described for Mercury (e.g., Watters et al., 2001; Watters, 2021). Several of the authors assigned each landform a lobate scarp or wrinkle ridge designation by visual inspection and then compared their assignments. Transitional structures could also be categorized as either wrinkle ridges or lobate scarps at the location of the profile showing the highest structural relief that was also used to collect our measurements. Following Byrne et al. (2014), we also categorized the shortening landforms as cratered-plains structures or smooth-plains structures.

All landforms were assigned to one of five map patterns: concave, sinuous, straight, convex, or switching vergence. Convexity and concavity were defined with respect to the hanging wall block. In a concave map pattern (Fig. 3a), the hanging wall creates a concave scarp shape over the footwall; the concave pattern opens towards the footwall. Sinuous map patterns (Fig. 3b) demonstrate a large amount of variation along strike as the surface break pattern switches between concave and convex patterns along the length of the structure. Straight map patterns (Fig. 3c) show little curvature or variability along the length of the surface break. Convex map patterns (Fig. 3d) depict the hanging wall extending in an arching manner over the footwall, such that the concave pattern opens towards the hanging wall (often described as an arcuate or bow pattern (e.g., Watters et al., 2015; Byrne et al., 2018)). Shortening landforms that have a switching vergence map pattern (Fig. 3e) demonstrate tectonic movement in opposite directions along the length of the structures; that is, the hanging wall and footwall switch sides along the structure’s length.

In ArcMap, each landform was analyzed using a stereographic projection centered on the landform. We mapped their surface breaks at a 1:250,000 scale as polylines using the streaming function with vertex placements every 500 m. Marker points were placed every 10 km along the polylines/surface breaks, and topographic profiles were generated perpendicular to the landform at these marker points. Points that comprise the profile were evenly spaced every 245 m along the length as this is approximately the same as the highest resolution DEMs used in this work. All topographic profiles along a landform were compared to determine which profile displayed the maximum structural relief. Morphological measurements were made along the profile with maximum structural relief.

We measured and calculated twelve parameters on each shortening landform (Fig. 4). The structural relief (in meters) is the elevation difference measured between the onset of the forelimb/surface break and

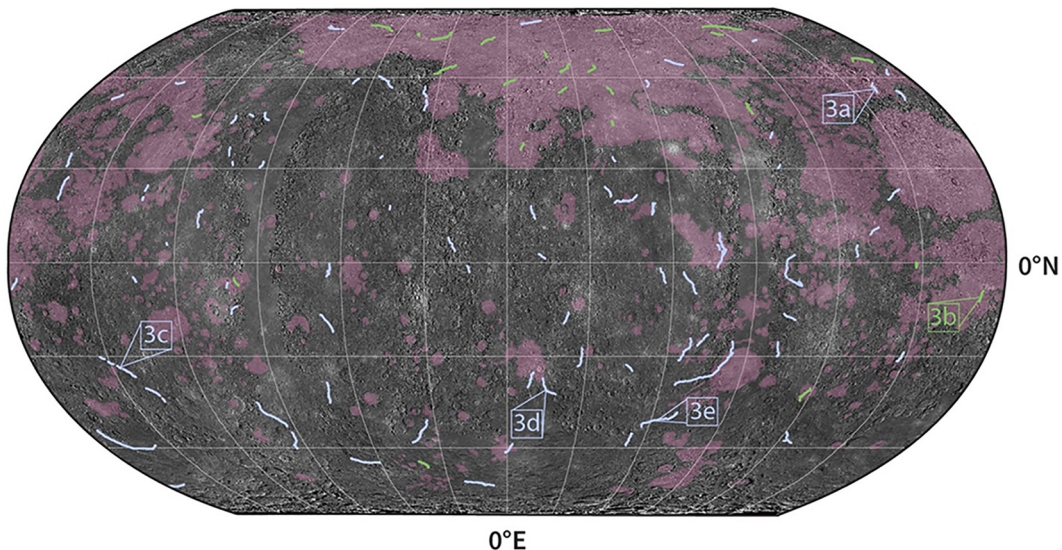


Fig. 2. Global map of Mercury in Robinson projection, showing the 100 shortening landforms analyzed in this study. Those that were traditionally identified as lobate scarps are shown in light blue, while those identified as wrinkle ridges are shown in green. Smooth-plains units (Denevi et al., 2013) are highlighted in pink. The map indicates the locations of five examples of shortening landforms, shown in Fig. 3 (a-e). (For interpretation of the references to colour in this figure legend, the reader is referred to the web version of this article.)

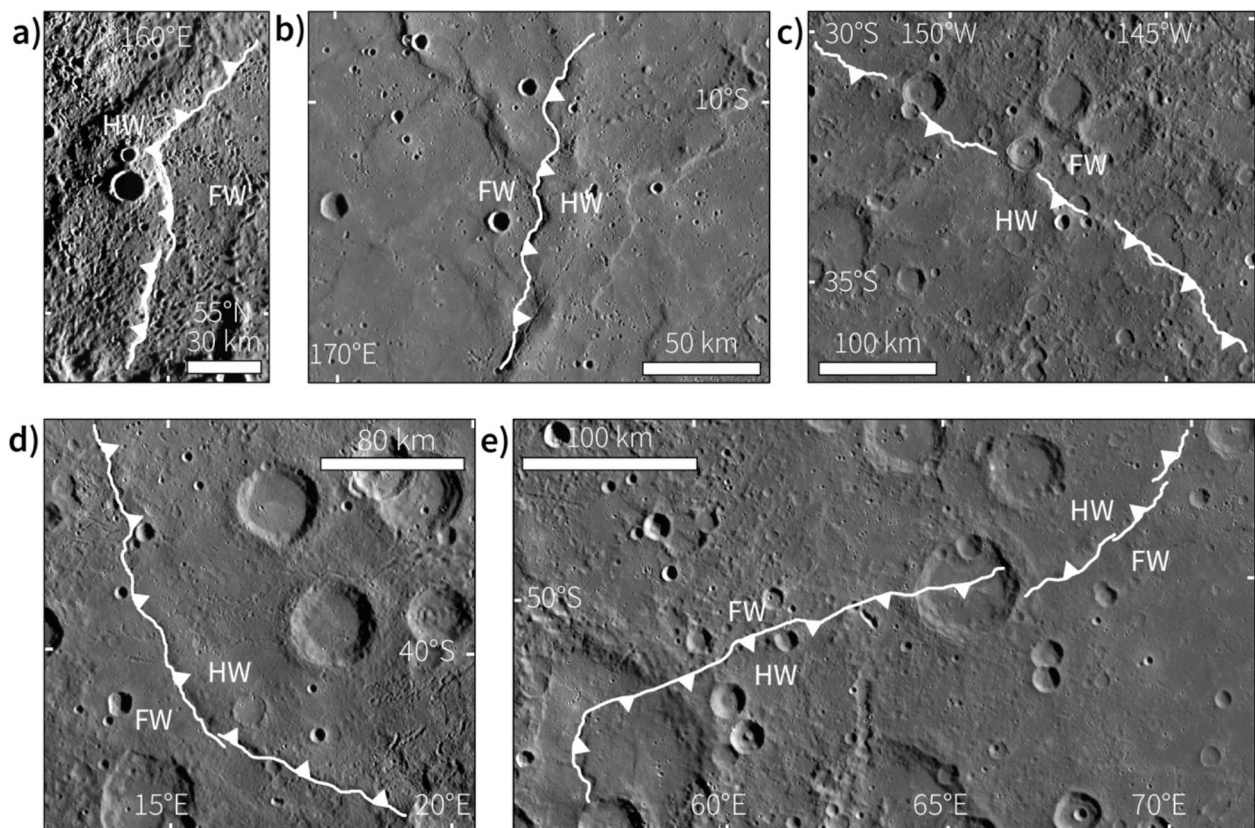


Fig. 3. Examples of the five scarp map patterns observed in this study. Here, the hanging walls are denoted with 'HW' and the footwalls are labeled with 'FW'. a) A scarp with a concave map trace. b) A scarp with a sinuous map trace. c) A scarp with a straight map trace. d) A scarp with a convex map pattern. e) A scarp for which vergence switching is evident. All images are shown in a stereographic projection centered on the shortening landform.

the peak of the topographic profile. The *breadth* (meters) of the structure is the horizontal distance across the topographic profile measured from the surface break to the end of the backlimb (Fig. 4), with the end of the backlimb being that point where the structure is no longer topographically distinguishable from the surrounding terrain. The breadth thus

represents the final length of the transect after shortening occurred. *Total cross-sectional length* (meters) is the distance along the transect (Fig. 4) and represents the initial length of the transect before shortening. *Shortening strain* (unitless) along the transect is the change in length (breadth minus total cross-sectional length) divided by the total

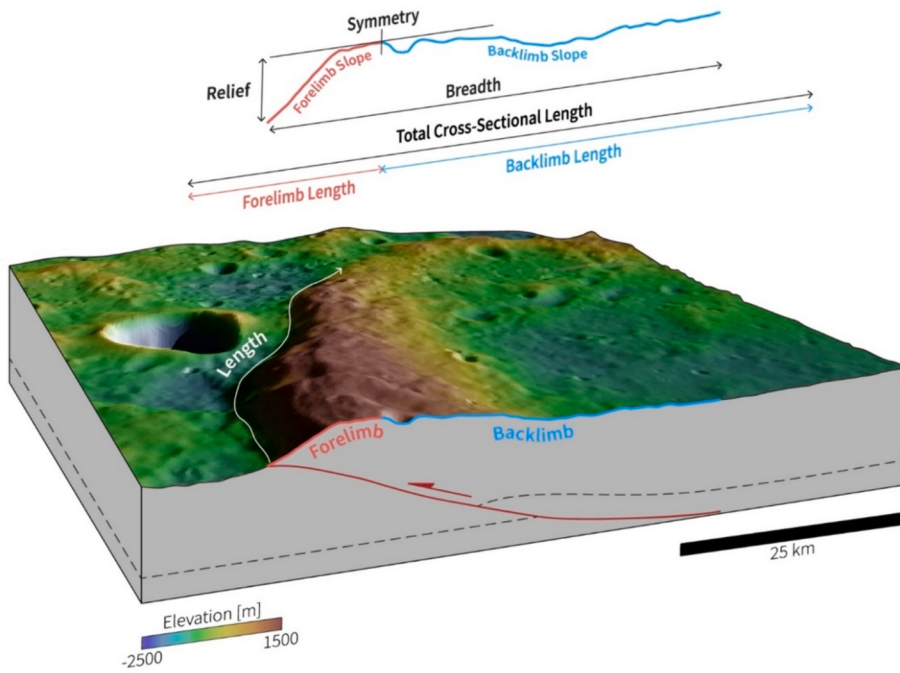


Fig. 4. Block diagram of a shortening landform annotated with parameters measured for each landform in Fig. 2. The landform shows the shape of the forelimb (in red) and backlimb (in blue) and part of the map trace (in white) along which the fault length was measured. The extracted profile with the maximum relief shows the breadth and locations where symmetry and slopes of the forelimb and backlimb were derived. The horizontal lines labeled Forelimb Length, Backlimb Length, and total Cross-Sectional Length are representations of the unfolded topographic profile. Thrust fault geometry in the subsurface is interpreted based on the morphology of the structure. The assumed fault geometry is based on simple cross-sectional balancing, and similar fault structures generated in previous modeling studies (e.g., Herrero-Gil et al., 2019). The dashed line in the subsurface represents an arbitrary marker horizon to depict deformation along the fault. The image in this figure is taken from the low-incident angle global mosaic. Elevation (Bertone et al., 2023) is shown as blue for low-lying areas and brown for high-standing terrain. (For interpretation of the references to colour in this figure legend, the reader is referred to the web version of this article.)

cross-sectional length, under the assumption that the total cross-sectional length is the initial length that was shortened entirely by the underlying thrust fault to the presently observed breadth. *Forelimb length* (meters) is the component of the total cross-sectional length measured from the surface break to the peak of the shortening landform, and *backlimb length* (meters) is the component of the total cross-sectional length measured from the peak of the topographic profile to the end of the backlimb.

Forelimb slope (measured in degrees, Fig. 4) is the average slope between each pair of adjacent points along the transect from the surface break to the peak of the shortening landform. The same method was applied to find the *backlimb slope* (degrees). The forelimb generally slopes upwards, and thus has positive slope values, whereas the backlimb generally slopes down and thus has negative slope values. *Symmetry* (degrees) is the difference of the forelimb slope and absolute value of the backlimb slope. A symmetrical shortening landform will have a symmetry of 0°, whereas deviations from 0° represent asymmetrical landforms. *Percent backlimb downslope* is the ratio of down-sloping (negative) backlimb slope segments to the total number of backlimb slope segments in the profile. A backlimb that slopes downward everywhere will have a percent downslope of 100%. This metric captures the complexity of topography on the backlimb, such as the "wrinkle" on wrinkle ridges.

The *length* (meters) of the shortening landform was identified using the mapped traces of the scarps and ridges (Fig. 2). To avoid distortions from the projection of global data, we used the Tools for Graphics and Shapes Plugin for ArcMap 10.8 to calculate geodesic lengths. The block diagram in Fig. 4 shows half of the length of the shortening landform.

To test if our measurements are biased by dependencies of landform size on terrain ruggedness or DEM resolution, we also calculated the *Topographic Roughness Index (TRI)*, given by Riley et al. (1999) as:

$$\text{TRI} = \sqrt{\frac{1}{N} \sum_{i=1}^N (x_i - \bar{x})^2},$$

where N is the number of transect segments measured along the topographic profile, and x_i is the elevation at segment i on the profile.

2.2. Statistical analysis

We performed two types of statistical analyses to assess the existence of distinct categories of morphologic shortening landforms: a principal component analysis (PCA) and a linear discriminant analysis (LDA), a type of discriminant function analysis. As for all statistical techniques, these analyses assume random sampling. PCA and LDA also assume multivariate normality, which is achieved through data transformations of some variables (see Table A1). After the data were transformed, they were scaled by the z-score of each measurement: $z = (x - \mu)/\sigma$, where x is the measurement, μ is the average of the measurements, and σ is the standard deviation. This transformation places each measurement on the same scale with a mean of zero and a standard deviation of one, causing the LDA to be influenced purely by the variance of the data and not by the relative size of different measurements.

PCA is an eigenanalysis-based multivariate statistical method for rotating the data along orthogonal axes that explain a progressively decreasing proportion of the variance (i.e., principal components, PCs; Pearson, 1901). By selecting the PCs that explain the greatest proportion of the total variance, PCA can be used to reduce dimensionality and simplify analysis of multivariate data. For this study, these PCs can be used to detect whether the landforms cluster into distinct categories or lie along a continuum. Each PC is described by a set of linear coefficients called loadings that describe how much each variable contributes to

each PC. Through these loadings, we can determine which morphologic characteristics account for the greatest variance in Mercury's shortening landforms.

Linear discriminant analysis constructs a linear mathematical model that maximizes the separation between predefined groups using eigenanalysis methods (Davis, 2002; Maindonald and Braun, 2003). LDA generates $k - 1$ linear discriminants (LDs), where k is the number of predefined groups (landform categories or terrain types). Each sample has scores (positions) along these linear discriminants, and the positions of samples in this linear discriminant space is used to classify the samples into groups. If the model can successfully classify the samples into groups based on the morphological variables, the landform categories assigned by LDA will match those that we assigned during data collection.

We conducted two LDAs with two groups, one distinguishing lobate scarps and wrinkle ridges, the other distinguishing smooth-plains and cratered-plains structures. Once an LDA model was completed, it was evaluated using a “jackknife” validation technique with the original data to reduce the self-constructed biasing accuracy of the model. The jackknife technique is a resampling method in which a statistic—in our case, the results of running our sample through our LDAs—is calculated repeatedly with one of the observations excluded in turn. By calculating the statistic multiple times, an estimate of the parameter, or average of how accurate the LDA is, can be found.

3. Results

A catalog of 100 shortening landforms was compiled that contains the geographic position of each shortening landform, the highest-resolution DEM available at the time of this writing that covers the shortening landform, the 12 collected parameters, the visual assessment of the traditional category to which the shortening landform ought to be assigned, the map patterns of the scarp (Fig. 3), and the terrain type in which the structure is found. The catalog comprises 75 lobate scarps and 25 wrinkle ridges, and is included in the supplementary material (Loveless et al., 2024).

3.1. Principal component analysis

For our PCA, Appendix Fig. 1 shows the scree plot that presents the percentage of variance that is explained by each of the 12 PCs. PCs 1 and 2 together describe 65% of the variance of the data, and therefore we use them to present and discuss the results for grouping of shortening landforms. Variable loadings (Table 1, columns PC1 and PC2) describe the contribution of each variable to each principal component. A positive loading has a positive correlation with its respective PC and likewise a negative loading is negatively correlated. Loadings for each PC were deemed important contributors if their absolute value exceeded the value of a loading if each loading contributed equally to the variance of a

PC, i.e., given by $\sqrt{1/\# \text{of measurements}}$ (see the bold values in Table 1). The strongest influencing parameters on PC1 are those that pertain to the size of the shortening landforms, i.e., relief, breadth, total cross-sectional length, fore- and backlimb length, and mapped length (Table 1). PC2 is most influenced by the shortening strain and both fore- and backlimb slopes; however, as shown below, TRI value, breadth, and cross-sectional length are also influential (Table 1).

PCA sample scores form a single cloud of points (Fig. 5). These scores are coded in three ways to aid in the interpretation of the PCs (Fig. 5), including the traditional categories for a clustering of lobate scarps and wrinkle ridges (Fig. 5a), concave, convex, straight, sinuous, and switching verge map patterns (Fig. 5b), and cratered-plains structures and cratered-plains structures (i.e., those shortening landforms classified solely by terrain type) (Fig. 5c). For each categorization, there is substantial overlap in categories with no distinct separation of groups. This indicates that the morphology of shortening landforms on Mercury provides no evidence of any distinct groups based on traditional categories, map pattern, or terrain type.

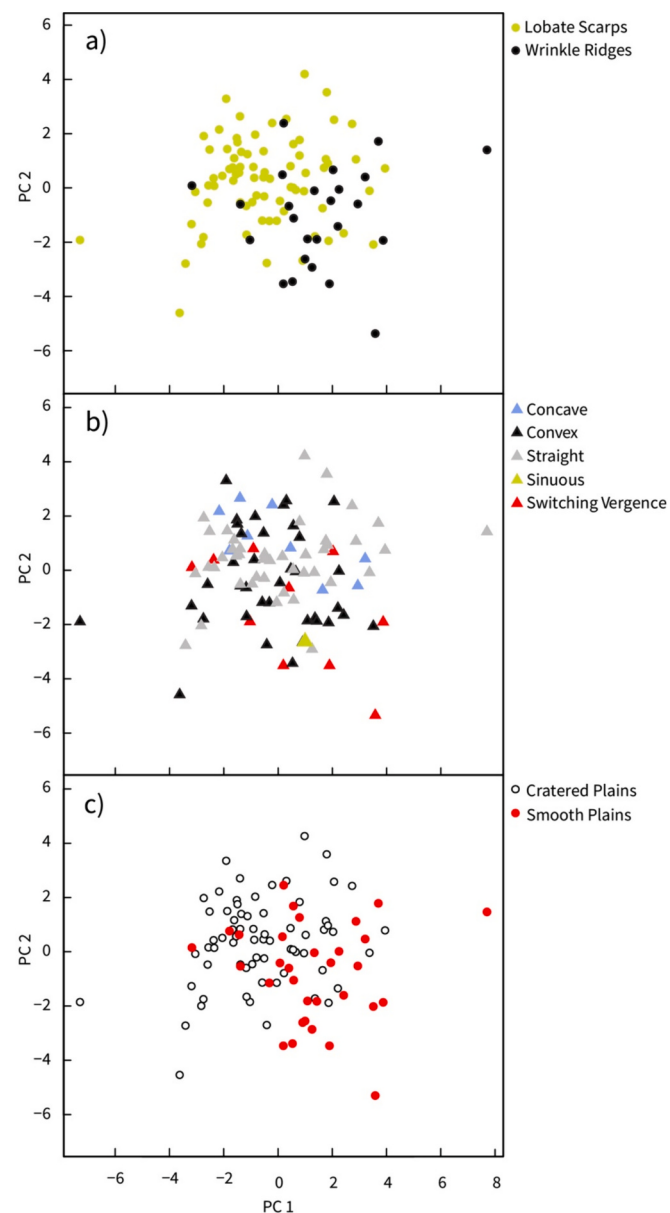


Fig. 5. PCA sample scores coded by traditional categories (a), map trace (b), and (c) terrain type.

Table 1

Loadings of variables on PCs 1 and 2 and linear discriminant loadings for the traditional category LDA (LD TC) and terrain type LDA (LD TT). Bolded values indicate the most important loadings for each axis.

Parameter	PC1	PC2	LD TC	LD TT
Relief	-0.38	0.26	-3.70	-2.87
Breadth	-0.43	-0.18	-28.97	-39.81
Total Cross-Sectional Length	-0.43	-0.18	26.79	42.68
Shortening Strain	-0.12	0.50	-0.15	0.72
Forelimb Slope	-0.16	0.48	1.70	0.41
Backlimb Slope	-0.05	0.43	0.17	-0.25
Symmetry	-0.20	0.29	0.13	0.49
Forelimb Length	-0.30	-0.17	2.81	0.63
Backlimb Length	-0.41	-0.14	1.41	-2.64
% Backlimb Downslope	0.13	0.09	-0.41	-0.10
Mapped Length	-0.32	-0.10	0.51	0.18
TRI	-0.17	0.21	0.27	0.04

3.2. Discriminant function analysis

LDA produces a linear equation that maximizes the separation of pre-defined groups. LDA loadings are the coefficients (slopes) in this linear equation. Their signs indicate the directions in which they influence a discriminant function, and their magnitudes indicates their relative contributions. Therefore, the sign of large loadings is important in assigning the relative extent of where the shortening landform would be placed in LD space. We performed LDAs to classify landforms by traditional types and terrain types (Table 1). For both the traditional categories and structures categorized by their host terrain, the breadth of the landform holds a strong negative influence on the LDA, whereas the total cross-sectional length holds an almost equally strong, positive influence on the LDA. In both cases, breadth and cross-sectional length are substantially more influential than any of the other measurements, and so they provide the greatest influence on the LDA predictions.

A jackknife resampling of the LDA indicates that it is 79% accurate in predicting the traditional categories of the shortening landforms. The LDA was 76% accurate in classifying landforms based on terrain type. Both LDAs were only moderately successful in predicting traditional categories and terrain types, and the 21–24% cases of inaccurate classification question the support of these classifications.

When a sample is assessed with an LDA, that sample is assigned an LD value that the LDA uses to distinguish the predefined group to which that sample belongs (Fig. 6). In an LDA that attempts to distinguish between two groups, samples that cannot be differentiated would have LD values in and around zero. Our traditional category LDA (Fig. 6a) assigns negative LD values to landforms where it predicts are lobate scarps, and positive LD values where it predicts wrinkle ridges. The negative and positive values produced by the terrain-type LDA correspond to predictions of cratered- and smooth-plains structures, respectively (Fig. 6b).

Both LDAs show a substantial overlap of categories between LD values, with many structures clustering near zero. The traditional category LDA assigns the landforms of this work with LDs that fall in the range of −2.33 to +4.60. Of this, a total of 67 structures are assigned LDs that fall in the range between −0.82 and +1.54. In this range, lobate scarp designations greatly extend over wrinkle ridge designations, indicating that the quantitative morphological measurements that define wrinkle ridges and lobate scarps are not distinctly different when assessed with this method. This result is emphasized by the misclassification of structures relative to our visual inspection (e.g., wrinkle ridges assigned negative-lobate scarp values Fig. 6b). The overlap of LDs implies that most shortening landforms exist on a spectrum between lobate scarps and wrinkle ridges, whereas the small remainder can be identified as distinguishable endmembers. In this work, 33 of the 100 structures are clear endmembers: just 25 lobate scarps and 8 wrinkle

ridges lie outside of this central cluster (Fig. 6).

The LDA pertaining to the terrain type in which the structures reside (Fig. 6b) also depicts a substantial amount of overlap between cratered-plains structures and smooth-plains structures, albeit with even fewer endmembers. This finding implies that the morphology of shortening landforms is not distinctly different across the terrains observed on Mercury's surface. All the structures in this study exist as either smooth-plains structures or cratered-plains structures (cf. Byrne et al., 2014), and so we interpret this result as indicating that a certain morphological variability of shortening landforms on Mercury is found in both terrain types. Unlike the traditional categories, however, categorization by terrain type does not assume specific morphological characteristics of shortening landforms, and so does not require (nor did we expect) the statistical detection of distinct groups based on morphology that were classified by Byrne et al. (2014) according to terrain type.

4. Discussion

We applied multivariate statistical analyses—principal component analysis and linear discriminant analyses—to assess if a systematic categorization of shortening landforms is possible based on morphological measurements alone. Prior to this study, shortening landforms on Mercury were assumed to fall into distinct categories based purely and subjectively on visual assessment of their map patterns and topography (Strom et al., 1975; Dzurisin, 1978; Melosh and McKinnon, 1988; Watters et al., 2004). Other studies have since challenged the use of these categories and have grouped Mercury's shortening landforms based on the terrain type in which they are located (e.g., Byrne et al., 2014). Although this latter approach is agnostic to landform morphology (and allows for the possibility that a continuum of landform shape exists), it sidesteps the issue of actually assessing quantitatively the morphology of shortening landforms on Mercury.

As with any statistical testing, it is important to note possible sources of bias and efforts for bias mitigation. One bias in our data collection may arise from the lack of equal and global coverage of high-resolution DEMs at present. This variability in data availability may bias our results towards larger landforms in more rugged terrain, such as cratered-plains landforms. We tested for dependency of landform size with terrain ruggedness by calculating the Topographic Roughness Index (TRI) along our profiles and observed its effect on our statistical results. The loadings of the TRI for both LDAs are negligible, whereas the loadings of the TRI for the PCA are small compared to the largest contributors (Table 1). A PCA performed without the TRI measurements (not included) produced nearly indistinguishable results. We take these results as support that our morphologic measurements are representative for a wide range of landform sizes on Mercury, irrespective of resolution and coverage of elevation data.

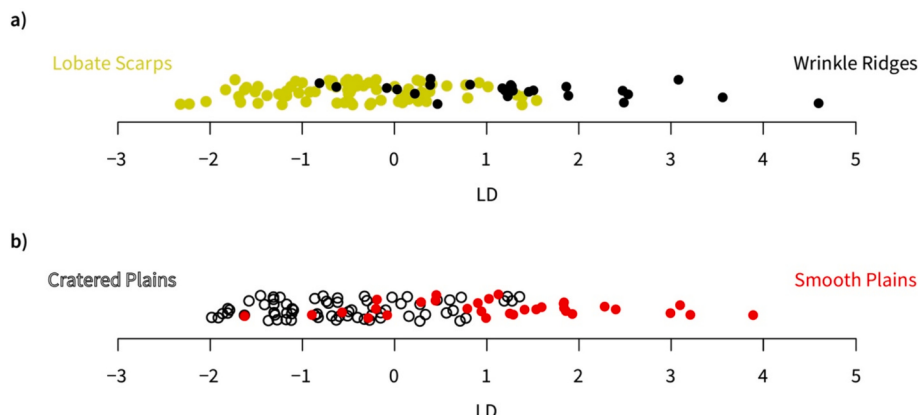


Fig. 6. Classification of landforms by linear discriminant analysis based on traditional categories (a) and terrain types (b). Note the poor discretization of landforms in both cases, suggesting that landform morphology does not support the existence of distinct categories per this technique.

Moreover, our data include shortening landforms spanning a wide range of sizes ($\sim 30\text{--}1000$ km in length), thus accounting for a wide range of structure size. We also tested for size bias by scaling relief to shortening landform length, and then plotting the scaled relief against the LDs generated by the LDAs. No correlation between relief-to-length ratio and the LDs was found. Additionally, we performed the LDAs without the breadth and topographic profile-length measurements, the most influential parameters in the original LDAs, to evaluate size bias. Excluding these data produced a similar spectrum rather than distinct groups: there was a substantial overlap in LD space for both the traditional categories and terrain type, and the success of the LDA correctly assigning the categories to our samples was approximately the same (80% and 73% for the traditional categories and terrain types respectively). These results indicate that additional evaluation of the LDA does not alter its outcome: the morphology of shortening landforms on Mercury does not separate such landforms into distinctly different groups.

4.1. “Lobate scarps” and “Wrinkle ridges”

Our principal component analysis and linear discriminant analyses demonstrate that morphological measurements do not support the grouping of shortening landforms on Mercury into distinctly different categories. Only one cluster of data points is displayed based on the sample scores created in our PCA, showing no distinct patterns within the data scatter. For shortening landforms classified into the traditional categories (Fig. 5a), our findings indicate that they are not distinctly different from one another for the morphologic parameters we assessed. PC1 is strongly anticorrelated with relief, breadth, total cross-sectional length, fore- and backlimb lengths, and mapped lengths (Table 1), implying that landform size may help in differentiating landform types. Although wrinkle ridge endmembers have generally lower relief than lobate scarps, there is substantial overlap of the two groups, with only few distinct lobate scarp and wrinkle ridge endmembers (note the lobate scarp and wrinkle ridge endmembers on the left and right of Fig. 5a, respectively). This finding indicates that the size of the landforms, as a function of their relief, breadth, and total cross-sectional length, does not unequivocally distinguish these categories. PC2 has a strong positive correlation with shortening strain and the slopes of the fore- and backlimb. Influential parameters on PC2 such as the slopes and shortening strain are measurements of a landform’s relative shape along its topographic profile, suggesting that the gradients of shortening landforms are also important in distinguishing landform type. However, lobate scarps and wrinkle ridges fully overlap along the PC2 axis, strongly implying that the parameters governing PC2 alone do not unequivocally distinguish between the traditional categories.

Principal component analysis is based only on the morphological measurements; it is agnostic to any group classification. In contrast, LDA constructs a linear model that maximizes the separation of pre-defined groups. In the LDA assessing the difference between lobate scarps and wrinkle ridges, higher (positive) LD values predicted a structure to be a wrinkle ridge, whereas lower (negative) LD values predict lobate scarps. Substantial overlap along the LD axis (Fig. 6a) highlights a broad region where lobate scarps and wrinkle ridges cannot be distinguished by this basis. Moreover, $\sim 20\%$ of structures are misclassified by a jackknife of the LDA. If lobate scarps and wrinkle ridges truly fell into distinct categories, there would be two clusters on opposite ends of the LD axis with little to no overlap and a minimum of false predictions. The LDA therefore supports the results of the PCA, indicating that although clear endmembers of what have been traditionally identified as “lobate scarps” and “wrinkle ridges” do exist, shortening landforms on Mercury form a spectrum between these morphologically idealized endmembers. This result is supported by observations of transitional structures (e.g., Watters and Nimmo, 2010; Clark et al., 2017; Watters, 2021) and by structures for which traditional classification is not obvious.

In the LDA, the total cross-sectional length and breadth are much

more influential than any other measurements (Table 1). This is an interesting outcome as both measurements give first-order estimates of the shortening caused by the faulting and folding of the structure. Breadth is particularly notable because it is governed by the geometry of the underlying thrust fault and associated folding (e.g., Brandes and Tanner, 2014). Specifically, shortening-landform breadth is influenced by a combination of fault and depth of penetration, and it may thus reflect a difference in the type of thrust system underlying the landforms (e.g., some examples in Boyer and Elliot, 1982; Martinez-Torres et al., 1994; Crane, 2020). Therefore, the distinction between lobate scarps and wrinkle ridges on Mercury may lie in the underlying thrust system structure rather than their morphology. Future studies should perform detailed analysis of the underlying fault geometries of lobate scarps and wrinkle ridges and compare the thrust systems of the two categories.

To visually assess the traditional categories, we first independently (i.e., individually) classified the thrust-fault related landforms and compared our heuristic assessments for each structure. In several instances, we debated our assessments of structures between our authorship group because our interpretations did not agree or because it was too difficult to decide between assigning only the terms lobate scarps and wrinkle ridges to landforms. The quantitative results of the PCA and LDA reflect this heuristic, qualitative ambiguity. Crane and Klimczak (2019) reached the same conclusion, confirming the finding stated in Byrne et al. (2018): “*a classification scheme for shortening structures based on morphology, such as that used historically for Mercury, works only in a general way but cannot capture the broad variation in geometry of these landforms*”.

One defining criterion of wrinkle ridges is the presence of a wrinkle that typically sits atop and frequently parallels the strike of the ridge (e.g., Strom et al., 1975; Dzurisin, 1978; Nahm et al., 2023). Of our 25 wrinkle ridges, 14 do not show this superimposed wrinkle and their categorization was based purely on the complex map pattern. Most shortening landforms on Mercury’s smooth plains have a wrinkle-ridge-like map pattern (Crane and Klimczak, 2019) but lack a clearly defined, superposed wrinkle that parallels the main ridge. Although small, wrinkle-like structures are widespread in the planet’s smooth plains, these structures are frequently not situated atop a broader ridge. That many ridges lack wrinkles may indicate that wrinkles did not form or that they are too degraded to be preserved—but speaks subjectively to the conclusion that not all wrinkle ridges are actually, in fact, wrinkle ridges.

While several thousands of shortening landforms have been mapped across Mercury’s surface ($n \approx 6000$, e.g., Byrne et al., 2014), only a few structures ($n \approx 60$) have been regarded as high-relief ridges (Watters, 2021). Due to this small sample size, high-relief ridges were not analyzed with the statistical methods presented in this study. High-relief ridges are noted to be more symmetrical in cross-section, as their general morphological characteristics resemble that of a lobate scarp aside from a steeper backlimb. Provided that symmetry and backlimb slope are not the most influential parameters in our statistical analyses (Table 1), and that high-relief ridges previously described in the literature are on the order of tens to hundreds of km in length (Watters, 2021)—which scales similarly to many shortening landforms in this work—we anticipate that high-relief ridges would lie in the shortening landform spectrum produced from our results, indistinguishable from the other traditional categories.

The traditional categories of shortening landforms have also been used for Mars (e.g., Watters and Robinson, 1999), the Moon (e.g., Watters, 1988), and Venus (e.g., Bilotti and Suppe, 1999). Our finding that morphology does not support the classification of landforms on Mercury into binary categories raises questions about the suitability of these classifications on other planetary bodies. In a recent study, McCullough (2023) focused on highlighting the differences between lobate scarps and wrinkle ridges on Mars by also conducting several LDAs based on morphology of shortening landforms there. Their LDA focused on surface observations also achieved only 79% accuracy, with

broad overlap between lobate scarp and wrinkle ridge morphology. These results largely match those in this study and suggest that shortening landforms on Mars also form a morphological spectrum defined by the “traditional” endmembers, further supporting that the retention of the existing, binary classification scheme obfuscates the complexity and natural variability that defines the real-world continuum of shortening landform morphologies.

4.2. Other categories

We also assessed if a distinct grouping of shortening landforms by terrain type can be statistically detected, as such groupings have been applied to Mercury (Byrne et al., 2014). Both the PCA and LDA showed that our landforms are not distinctly different from one another in different geological units across Mercury (Fig. 4c, 6b). There are eight endmembers for cratered-plains structures, which are the largest shortening landforms of our analysis. This finding supports the finding by Byrne et al. (2014) that the largest shortening landforms generally occur in Mercury’s cratered plains. However, our PCA shows that structure size or strain alone are not unequivocal criteria to distinguish smooth- and cratered-plains structures, especially when comparing landforms of intermediate and smaller sizes (≤ 600 km in length).

The substantial overlap of landforms in the LDA (Fig. 6b) with many structures having small absolute LD values shows that the morphology of shortening landforms do not differ distinctly by terrain type on Mercury. In particular, the loading of the TRI is very small (Table 1), indicating that terrain type does not influence the morphological variability on Mercury, particularly for attributes related to landform size and shape. However, as we note above, categorization by terrain type does not rely on morphologic characteristics of shortening landforms, and we therefore suggest that this classification scheme is appropriate so long as no assumptions are made regarding the morphology of the individual landforms themselves.

Finally, we also assessed if shortening landforms can be discretely categorized based on the map patterns they display (Figs. 3, 4b). Given the varying sample sizes between the five map patterns, a PCA was the only suitable method for assessing categories from map patterns. The PCA sample scores depict no distinct groupings based on map patterns, and all five patterns collectively form a single cloud of points. These results indicate that any shortening landform can exhibit any map pattern, regardless of various morphologic parameters such as those associated in PCs 1 and 2 with landform size and shape, or accumulated strain amount.

5. Conclusions

Shortening landforms on Mercury have been traditionally classified into three categories: lobate scarps, wrinkle ridges, and high-relief ridges. This distinction has primarily been based on subjective, visual

assessment of structures in photogeologic datasets. The goal of this study was to assess if the traditional classification scheme for shortening landforms on Mercury can be applied based on the morphologic variability using multivariate statistical tests. We find that the morphology of most shortening landforms on Mercury is consistent with elements of both wrinkle ridges and lobate scarps, with few distinct endmembers of either category. We also find that any morphology of shortening landforms can be observed in any terrain type and that the different observed map patterns can belong to any shortening landform regardless of its morphology.

In conclusion, the terms “lobate scarp,” “wrinkle ridge,” and “high-relief ridge,” although having found widespread use in planetary tectonics literature (e.g., Melosh and McKinnon, 1988; Watters and Robinson, 1999; Watters et al., 2004), do not adequately capture the variability of shortening landform shape, and can erroneously undermine the true complexity of such landforms. The continued use of these terms will hamper the facilitation of new insights into the geometry of crustal shortening on rocky planetary bodies and may reduce the accessibility of planetary tectonics to those who study shortening systems on Earth—where such terms have never been routinely used.

CRediT authorship contribution statement

Stephan R. Loveless: Writing – original draft, Methodology, Investigation, Formal analysis. **Christian Klimczak:** Writing – review & editing, Supervision, Methodology, Funding acquisition, Conceptualization. **Leta R. McCullough:** Writing – review & editing, Validation, Investigation. **Kelsey T. Crane:** Writing – review & editing, Methodology, Funding acquisition, Conceptualization. **Steven M. Holland:** Writing – review & editing, Formal analysis. **Paul K. Byrne:** Writing – review & editing, Funding acquisition, Conceptualization.

Declaration of competing interest

The authors declare that they have no known competing financial interests or personal relationships that could have appeared to influence the work reported in this paper.

Data availability

The supplementary material for this research is available in Loveless et al. (2024): <https://data.mendeley.com/datasets/8968vkpgds/2>.

Acknowledgements

We thank Seiji Sugita for their editorial assistance as well as Lisa Schleicher and an anonymous reviewer for their helpful suggestions. This research was supported by NASA’s Solar System Workings program under grant 20-SSW20-0153.

Appendix A. Appendix

Appendix Table 1

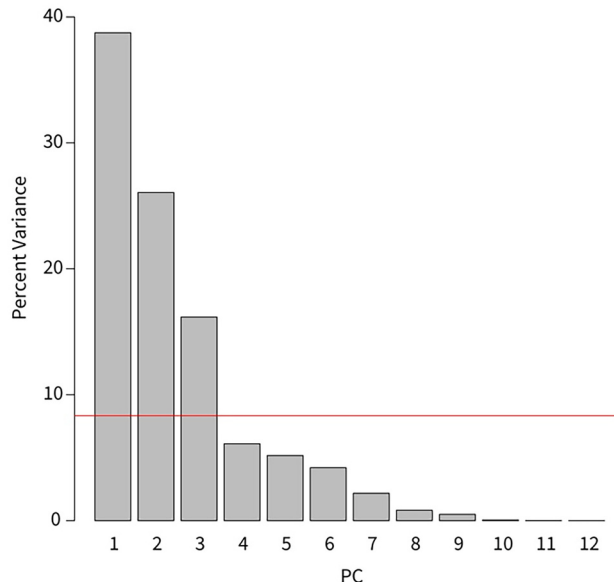
Transformations used to normalize all of the measurements in this study. After these transformations, the data was scaled using the measurement’s z -scores (where $z = (x - \mu)/\sigma$).

Parameter	Normalized Transformation
Relief	$\ln(x)$
Breadth	$\ln(x)$
Total Cross-Sectional Length	$\ln(x)$
Shortening Strain	$\ln(x)$
Forelimb Slope	$\ln(x)$

(continued on next page)

Appendix Table 1 (continued)

Parameter	Normalized Transformation
Backlimb Slope	$\ln(-x)$
Symmetry	$\ln(x)$
Forelimb Length	$\ln(x)$
Backlimb Length	$\ln(x)$
% Backlimb Downslope	$\ln(x)$
Mapped Length	$\ln(x)$
TRI	$\ln(x)$



Appendix Fig. 1. Scree plot depicting the percent variance described by each of the 12 principal components. The red horizontal line depicts the percent variance each PC would have if they each equally contributed to the total variance observed across the data (i.e., 100% variance/12 parameters).

References

- Becker, K.J., Robinson, M.S., Becker, T.L., Weller, L.A., Edmundson, K.L., Neumann, G.A., Perry, M.E., Solomon, S.C., 2016. First global digital elevation model of Mercury. In: *Lunar Planet. Sci. XLVII. Abstract*, p. 2959.
- Bertone, S., Mazarico, E., Barker, M.K., Siegler, M.A., Martinez-Camacho, J.M., Hamill, C.D., Glantzberg, A.K., Chabot, N.L., 2023. Highly resolved topography and illumination at Mercury's south pole from MESSENGER MDIS NAC. *Planet. Sci. J.* 4, 21. <https://doi.org/10.3847/psj/acaddb>.
- Bilotti, F., Suppe, J., 1999. The global distribution of wrinkle ridges on Venus. *Icarus* 139, 137–157. <https://doi.org/10.1006/icar.1999.6092>.
- Boyer, S.E., Elliot, D., 1982. Thrust systems. *AAPG Bull.* 66 <https://doi.org/10.1306/03b5a77d-11d7-8645000102c1865d>.
- Brandes, C., Tanner, D.C., 2014. Fault-related folding: a review of kinematic models and their application. *Earth Sci. Rev.* 138, 352–370. <https://doi.org/10.1016/j.earscirev.2014.06.008>.
- Byrne, P.K., Klimczak, C., Şengör, A.M.C., Solomon, S.C., Watters, T.R., Hauck II, S.A., 2014. Mercury's global contraction much greater than earlier estimates. *Nat. Geosci.* 7, 301–307. <https://doi.org/10.1038/ngeo2097>.
- Byrne, P.K., Klimczak, C., LaFond, J.K., 2016. The East Kaibab monocline: A Terran lobate scarp?. In: *Lunar Planet. Sci. XLVII. Abstract*, p. 1022.
- Byrne, P.K., Klimczak, C., Şengör, A., 2018. The tectonic character of Mercury. In: Solomon, S.C. (Ed.), *Mercury. The View after MESSENGER*, pp. 249–286.
- Clark, J.D., van der Bogert, C.H., Hiesinger, H., Bernardt, H., 2017. Wrinkle ridge-lobate scarp transition of West Serenitatis: Indications for recent tectonic activity. In: *Lunar Planet. Sci. XLVIII. Abstract*, p. 1001.
- Crane, K., 2020. Approach and application of industry software to structural investigations in the subsurface of Mercury's thrust fault-related landforms. *J. Struct. Geol.* 141, 104218 <https://doi.org/10.1016/j.jsg.2020.104218>.
- Crane, K.T., Klimczak, C., 2017. Timing and rate of global contraction on Mercury. *Geophys. Res. Lett.* 44, 3082–3089. <https://doi.org/10.1002/2017gl072711>.
- Crane, K.T., Klimczak, C., 2019. Tectonic patterns of shortening landforms in Mercury's northern smooth plains. *Icarus* 317, 66–80. <https://doi.org/10.1016/j.icarus.2018.05.034>.
- Davis, J.C., 2002. *Statistics and Data Analysis in Geology*, Third edition. John Wiley and Sons. ISBN: 978-0-471-17275-8.
- Denevi, B.W., Robinson, M.S., Solomon, S.C., Murchie, S.L., Blewett, D.T., Domingue, D.L., McCoy, T.J., Ernst, C.M., Head, J.W., Watters, T.R., Chabot, N.L., 2009. The evolution of Mercury's crust: a global perspective from MESSENGER. *Science* 324, 613–618. <https://doi.org/10.1126/science.1172226>.
- Denevi, B.W., Ernst, C.M., Meyer, H.M., Robinson, M.S., Murchie, S.L., Whitten, J.L., Head, J.W., Watters, T.R., Solomon, S.C., Ostrach, L.R., Chapman, C.R., Byrne, P.K., Klimczak, C., Peplowski, P.N., 2013. The distribution and origin of smooth plains on Mercury. *J. Geophys. Res. Planets* 118, 891–907. <https://doi.org/10.1002/jgre.20075>.
- Dzurisin, D., 1978. The tectonic and volcanic history of Mercury as inferred from studies of scarps, ridges, troughs, and other lineaments. *J. Geophys. Res. Solid Earth* 83, 4883–4906. <https://doi.org/10.1029/jb083ib10p04883>.
- Golombek, M.P., Plescia, J.B., Franklin, B.J., 1991. Faulting and folding in the formation of planetary wrinkle ridges. *Proc. Lunar Planet. Sci.* 21, 679–693. <https://ui.adsabs.harvard.edu/abs/1991LPSC...21..679G>.
- Golombek, M.P., Anderson, F.S., Zuber, M.T., 2001. Martian wrinkle ridge topography: evidence for subsurface faults from MOLA. *J. Geophys. Res.: Planets* 106, 23811–23821. <https://doi.org/10.1029/2000je001308>.
- Head, J.W., Chapman, C.R., Strom, R.G., Fassett, C.I., Denevi, B.W., Blewett, D.T., Ernst, C.M., Watters, T.R., Solomon, S.C., Murchie, S.L., Prockter, L.M., Chabot, N.L., Gillis-Davis, J.J., Whitten, J.L., Goudge, T.A., Baker, D.M.H., Hurwitz, D.M., Ostrach, L.R., Xiao, Z., Merline, W.J., Kerber, L., Dickson, J.L., Oberst, J., Byrne, P.K., Klimczak, C., Nittler, L.R., 2011. Flood volcanism in the northern high latitudes of Mercury revealed by MESSENGER. *Sci. (N. York, NY)* 333, 1853–1856. <https://doi.org/10.1126/science.1211997>.
- Herrero-Gil, A., Ruiz, J., Romeo, I., 2019. 3D modeling of planetary lobate scarps: the case of Ogygis Rupes. *Mars. Earth Planet. Sci. Lett.* 532, 116004 <https://doi.org/10.1016/j.epsl.2019.116004>.
- Klimczak, C., Kling, C.L., Byrne, P.K., 2018. Topographic expressions of large thrust faults on Mars. *J. Geophys. Res. Planets* 123, 1973–1995. <https://doi.org/10.1029/2017je005448>.
- Loveless, S., Klimczak, C., McCullough, L., Crane, K., Holland, S., Byrne, P., 2024. Code and Data for 'A statistical evaluation of the morphological variability of shortening landforms on Mercury.' Revised, Mendeley Data V2. <https://doi.org/10.17632/8968vkpgpd.2>.
- Maindonald, J., Braun, W.J., 2003. *Data Analysis and Graphics Using R – an Example-Based Approach*, Third edition. ISBN-13 978-0-511-71286-9.
- Martinez-Torres, L.M., Ramon-Lluch, R., Eguiluz, L., 1994. Tectonic wedges: geometry and kinematic interpretation. *J. Struct. Geol.* 16, 1491–1494. [https://doi.org/10.1016/0191-8141\(94\)90011-6](https://doi.org/10.1016/0191-8141(94)90011-6).

- McCullough, L., 2023. Morphological and structural characterization of shortening landforms on Mars. Mississippi State University theses and dissertations, p. 6025. <https://scholarsjunction.msstate.edu/td/6025>.
- Melosh, H.J., McKinnon, W.B., 1988. The tectonics of Mercury. In: Vilas, F., Chapman, C.R., Matthews, M.S. (Eds.), *Mercury*, pp. 374–400.
- Mueller, K., Golombek, M., 2004. Compressional structures on Mars. *Earth Planet. Sci. Lett.* 23, 435–464. <https://doi.org/10.1146/annurev.earth.32.101802.120553>.
- Nahm, A.L., Watters, T.R., Johnson, C.L., Banks, M.E., van der Bogert, C.H., Weber, R.C., Andrews-Hanna, J.C., 2023. Tectonics of the moon. *Rev. Mineral. Geochem.* 89, 691–727. <https://doi.org/10.2138/rmg.2023.89.16>.
- Okubo, C.H., Schultz, R.A., 2004. Mechanical stratigraphy in the western equatorial region of Mars based on thrust fault-related fold topography and implications for near-surface volatile reservoirs. *GSA Bull.* 116, 594–605. <https://doi.org/10.1130/b25361.1>.
- Pearson, K., 1901. LIII. On lines and planes of closest fit to systems of points in space. *Philos. Mag. Ser.* 6 2, 559–572. <https://doi.org/10.1080/14786440109462720>.
- Plescia, J.B., Golombek, M.P., 1986. Origin of planetary wrinkle ridges based on the study of terrestrial analogs. *GSA Bull.* 97, 1289–1299. [https://doi.org/10.1130/0016-7606\(1986\)97<1289:oopwrb>2.0.co;2](https://doi.org/10.1130/0016-7606(1986)97<1289:oopwrb>2.0.co;2).
- Preusker, F., Oberst, J., Head, J.W., Watters, T.R., Robinson, M.S., Zuber, M.T., Solomon, S.C., 2011. Stereo topographic models of Mercury after three MESSENGER flybys. *Planet. Space Sci.* 59, 1910–1917. <https://doi.org/10.1016/j.pss.2011.07.005>.
- Riley, S.J., DeGloria, S.D., Elliot, R., 1999. A terrain ruggedness index that quantifies topographic heterogeneity. *Int. J. Therm. Sci.* 5 (1–4), 23–27.
- Schleicher, L.S., Watters, T.R., Martin, A.J., Banks, M.E., 2019. Wrinkle ridges on Mercury and the moon within and outside of mascons. *Icarus* 331, 226–237. <https://doi.org/10.1016/j.icarus.2019.04.013>.
- Schultz, R.A., 2000. Localization of bedding plane slip and backthrust faults above blind thrust faults: keys to wrinkle ridge structure. *J. Geophys. Res. Planets* 105, 12035–12052. <https://doi.org/10.1029/1999je001212>.
- Schultz, R.A., Watters, T.R., 2001. Forward mechanical modeling of the Amenthes Rupes thrust fault on Mars. *Geophys. Res. Lett.* 28, 4659–4662. <https://doi.org/10.1029/2001gl013468>.
- Solomon, S.C., 1977. The relationship between crustal tectonics and internal evolution in the moon and Mercury. *Phys. Earth Planet. Inter.* 15, 135–145. [https://doi.org/10.1016/0031-9201\(77\)90026-7](https://doi.org/10.1016/0031-9201(77)90026-7).
- Solomon, S.C., 1978. On volcanism and thermal tectonics on one-plate planets. *Geophys. Res. Lett.* 5, 461–464. <https://doi.org/10.1029/gl005i006p00461>.
- Solomon, S.C., Smrekar, S.E., Bindschadler, D.L., Grimm, R.E., Kaula, W.M., McGill, G.E., Phillips, R.J., Saunders, R.S., Schubert, G., Squyres, S.W., Stofan, E.R., 1992. Venus tectonics: an overview of Magellan observations. *J. Geophys. Res. Planets* 97, 13199–13255. <https://doi.org/10.1029/92je01418>.
- Squyres, S.W., Jankowski, D.G., Simons, M., Solomon, S.C., Hager, B.H., McGill, G.E., 1992. Plains tectonism on Venus: the deformation belts of Lavinia Planitia. *J. Geophys. Res.: Planets* 97, 13579–13599. <https://doi.org/10.1029/92je00481>.
- Strom, R.G., 1979. Mercury: a post-mariner 10 assessment. *Space Sci. Rev.* 24, 3–70. <https://doi.org/10.1007/bf00221842>.
- Strom, R.G., Trask, N.J., Guest, J.E., 1975. Tectonism and volcanism on Mercury. *J. Geophys. Res. Solid Earth* 80, 2478–2507. <https://doi.org/10.1029/jb080i017p02478>.
- Trask, N.J., Guest, J.E., 1975. Preliminary geologic terrain map of Mercury. *J. Geophys. Res.* 80, 2461–2477. <https://doi.org/10.1029/jb080i017p02461>.
- Watters, T.R., 1988. Wrinkle ridge assemblages on the terrestrial planets. *J. Geophys. Res. Solid Earth* 93, 10236–10254. <https://doi.org/10.1029/jb093ib09p10236>.
- Watters, T.R., 1993. Compressional tectonism on Mars. *J. Geophys. Res.* 98, 17049. <https://doi.org/10.1029/93je01138>.
- Watters, T.R., 2003. Lithospheric flexure and the origin of the dichotomy boundary on Mars. *Geology* 31, 271–274. [https://doi.org/10.1130/0091-7613\(2003\)031<0271:lfatoo>2.0.co;2](https://doi.org/10.1130/0091-7613(2003)031<0271:lfatoo>2.0.co;2).
- Watters, T.R., 2021. A case for limited global contraction of Mercury. *Commun. Earth Environ.* 2, 9. <https://doi.org/10.1038/s43247-020-00076-5>.
- Watters, T.R., Nimmo, F., 2010. The tectonics of Mercury. In: Watters, T.R., Schultz, R.A. (Eds.), *Planetary Tectonics*, pp. 15–80. <https://doi.org/10.1017/cbo9780511691645.002>.
- Watters, T.R., Robinson, M.S., 1999. Lobate scarps and the Martian crustal dichotomy. *J. Geophys. Res.: Planets* 104, 18981–18990. <https://doi.org/10.1029/1998je001007>.
- Watters, T.R., Cook, A.C., Robinson, M.S., 2001. Large-scale lobate scarps in the southern hemisphere of Mercury. *Planet. Space Sci.* 49, 1523–1530. [https://doi.org/10.1002/0032-0633\(01\)00090-3](https://doi.org/10.1002/0032-0633(01)00090-3).
- Watters, T.R., Robinson, M.S., Bina, C.R., Spudis, P.D., 2004. Thrust faults and the global contraction of Mercury. *Geophys. Res. Lett.* 31 <https://doi.org/10.1029/2003gl019171>.
- Watters, T.R., James, P.B., Selvans, M.M., 2021. Mercury's crustal thickness and Contractual strain. *Geophys. Res. Lett.* 48, e2021GL093528 <https://doi.org/10.1029/2021gl093528>.
- Watters, T.R., Selvans, M.M., Banks, M.E., Hauck, S.A., Becker, K.J., Robinson, M.S., 2015. Distribution of large-scale contractual tectonic landforms on Mercury: Implications for the origin of global stresses. *Geophys. Res. Lett.* 42, 3755–3763. <https://doi.org/10.1002/2015gl063570>.
- Zuber, M.T., Smith, D.E., Phillips, R.J., Solomon, S.C., Neumann II, G.A., S.A.H. Peale, S.J., Barnouin, O.S., Head, J.W., Johnson, C.L., Lemoine, F.G., Mazarico, E., Sun, X., Torrence, M.H., Freed, A.M., Klimczak, C., Margot, J.-L., Oberst, J., Perry Jr., M.E., R.L.M. Balcerski, J.A., Michel, N., Talpe, M.J., Yang, D., 2012. Topography of the northern hemisphere of Mercury from MESSENGER laser altimetry. *Science* 336, 217–220. <https://doi.org/10.1126/science.1218805>.